Received: 28 August 2020 | Revised: 21 October 2020 | Accepted: 22 October 2020

DOI: 10.1111/jace.17581

Journal of the American Ceramic Society

ORIGINAL ARTICLE

Thermal depolarization and electromechanical hardening in Zn^{2+}-doped $Na_{1/2}Bi_{1/2}TiO_3$-$BaTiO_3$

Lalitha Kodumudi Venkataraman[1] | **Tingting Zhu**[1] | **Monica Pinto Salazar**[2] | **Kathrin Hofmann**[3] | **Aamir Iqbal Waidha**[1] | **J. C. Jaud**[1] | **Pedro B. Groszewicz**[2,4] | **Jürgen Rödel**[1]

[1]Department of Materials and Earth Sciences, Technical University of Darmstadt, Germany

[2]Institute of Physical Chemistry, Technical University of Darmstadt, Germany

[3]Eduard-Zintl-Institute of Inorganic and Physical Chemistry, Technical University of Darmstadt, Germany

[4]Department of Radiation Science and Technology, Delft University of Technology, Netherlands

Correspondence
Lalitha Kodumudi Venkataraman, Department of Materials and Earth Sciences, Technical University of Darmstadt, Germany.
Email: venkataraman@ceramics.tu-darmstadt.de

Funding information
Deutsche Forschungsgemeinschaft, Grant/Award Number: Grant No. BU 911/28-1 and KO 5948/1-1 (Nr. 414311761); Alexander von Humboldt Foundation, Grant/Award Number: 1-1, 414311761 and 28-1

Abstract

$Na_{1/2}Bi_{1/2}TiO_3$-based materials have been earmarked for one of the first large-volume applications of lead-free piezoceramics in high-power ultrasonics. Zn^{2+}-doping is demonstrated as a viable route to enhance the thermal depolarization temperature and electromechanically harden (1-*y*)$Na_{1/2}Bi_{1/2}TiO_3$-*y*$BaTiO_3$ (NBT100*y*BT) with a maximum achievable operating temperature of 150 °C and mechanical quality factor of 627 for 1 mole % Zn^{2+}-doped NBT6BT. Although quenching from sintering temperatures has been recently touted to enhance $T_{F\text{-}R}$, with quenching the doped compositions featuring an additional increase in $T_{F\text{-}R}$ by 17 °C, it exhibits negligible effect on the electromechanical properties. The effect is rationalized considering the missing influence on conductivity and therefore, negligible changes in the defect chemistry upon quenching. High-resolution diffraction indicates that Zn^{2+}-doped samples favor the tetragonal phase with enhanced lattice distortion, further corroborated by ^{23}Na Nuclear Magnetic Resonance investigations.

KEYWORDS

electromechanical hardening, $Na_{0.5}Bi_{0.5}TiO_3$, quenching, thermal depolarization, Zn^{2+}-doping

1 | INTRODUCTION

(1-*y*)$Na_{1/2}Bi_{1/2}TiO_3$-*y*$BaTiO_3$ (NBT100*y*BT) based material systems have been identified as a potential lead-free replacement in high-power ultrasonics.[1-4] Despite early reports on chemical modification in NBT-based materials[5,6] and indications of the potential for applications in high-frequency ultrasonics and as surface/bulk acoustic wave substrates[6,7], this material class received less attention due to the relatively poor piezoelectric properties in comparison with lead-based materials.[8,9] The recurrent debate on replacing lead-based materials in applications due to toxicity and environmental

concerns[1,2] led to revived interest in these materials. Research in this direction was further fueled by the demonstrated application of NBT-based material in ultrasonic cleaning[3] and superior high-power properties in comparison to Pb(Zr,Ti)O_3.[4] In the case of high-power applications, both high thermal stability of the piezoelectric properties and high mechanical quality factor (Q_m) are required.[1] NBT6BT is a non-ergodic relaxor exhibiting pseudocubic symmetry. Upon application of electric field, NBT6BT transforms into a phase mixture of rhombohedral and tetragonal phases.[10] The thermal stability of the ferroelectric state in NBT-based materials is dictated by the ferroelectric-relaxor transformation temperature (T_{F-R}), the temperature at which the material loses its long-range ordered ferroelectricity. The depolarization temperature (T_d) at which the material loses its piezoelectricity is governed by T_{F-R} in the absence of any external stimuli. NBT6BT depolarizes at ~100 °C[7] and exhibits a Q_m of 150.[11,12] Several strategies like doping[13-15], grain-size refinement[16], formation of composites[17], and quenching[18,19] have been adopted to enhance T_d and/or the mechanical quality factor. Although several chemical modifications of NBT100*y*BT have been reported in the literature[15,20-24], the most promising approaches have been composite formation[17] and quenching.[18] In the case of the NBT6BT composites with ZnO inclusions, it was demonstrated that T_{F-R} can be increased up to 40 °C[25] with the maximum in Q_m of 420.[11] However, further development in this direction requires careful choice of the inclusions and the related mechanisms can be influenced by the diffusion of cations (e.g., Zn^{2+} from ZnO) from the inclusions into the NBT100*y*BT matrix phase.[26,27] Quenching results in a similar increase in T_{F-R} in NBT6BT[28], whereas for NBT9BT, the depolarization temperature was increased to 200 °C.[29] A drawback of the quenching approach is the development of residual stress in samples, which in extreme cases can result in fracture and limit this strategy in real-time applications.[19,30] None of the chemical modifications have resulted in a significant increase in both T_{F-R} and Q_m.[20-24,31-40] The best improvements were an increase in Q_m to ~600 with concurrent enhancement in T_{F-R} by 20 °C for 1 mole % Co_2O_3-added-85$(Na_{1/2}Bi_{1/2})TiO_3$–12$(K_{1/2}Bi_{1/2})TiO_3$–3$BaTiO_3$.[41] Fe- and Mn-doping were documented to increase T_{F-R} by 20 °C.[13,42] At the same time, increased electrical conductivity upon doping, especially in Fe-doped and off-stoichiometric compositions[42,43] raised concerns. In prior work, 4 mole % Zn^{2+}-doping was demonstrated to increase T_{F-R} by 40 °C.[15] However, the effects of Zn^{2+} substitution on electromechanical hardening were not reported. Until now, this report[15] provides the highest increase in T_{F-R} for doped NBT100*y*BT. Zn^{2+} is highly polarizable and therefore, could stabilize a long-range ferroelectric order, thus enhancing the thermal stability of the piezoelectric properties. Additionally, it is of interest to know the effects of Zn^{2+}-doping on the structural distortion of NBT100*y*BT, since, quenching[29] and grain size refinement[16] approaches correlate the enhanced T_{F-R} to the structural changes in the system.

With the above perspective, this study entails an investigation of the role of acceptor Zn^{2+}-doping on both T_{F-R} and electromechanical hardening in NBT100*y*BT. The Morphotropic Phase Boundary (MPB) of NBT-BT spans over a composition range with varying degree of average structural distortions. The composition with average pseudocubic (or very weak rhombohedral) distortion is referred to as the 'core-MPB' composition and the composition with average non-cubic (tetragonal) distortion at the MPB as 'end-member MPB', since it is close the tetragonal phase boundary in the composition-temperature phase diagram. Two different doping concentrations are investigated for a core-MPB (NBT6BT) and a tetragonal end-member MPB (NBT9BT) composition. A combination of local (^{23}Na Nuclear Magnetic Resonance, NMR) and global (diffraction) structural techniques is used to elucidate the influence of Zn^{2+}-doping on the enhanced tetragonal distortion and phase fraction and the consequent increase in thermal stability of the piezoelectric properties. In addition, the effect of Zn^{2+}-doping on the electrical conductivity is probed using impedance spectroscopy. Since quenching is also proposed as a promising route to enhance T_{F-R}, the doped compositions (0.5 mole % Zn) were also quenched and the electrical properties were characterized.

2 | EXPERIMENT

(1-*y*)$Na_{1/2}Bi_{1/2}TiO_3$-*y*$BaTiO_3$ (NBT100*y*BT) doped with *x* mole % ZnO (*y*=0.06, 0.09; *x*=0, 0.5 and 1) were prepared using the conventional solid-state reaction route. Here, *y* denotes the number of moles. Stoichiometric ratios of Na_2CO_3 (99.5%), $BaCO_3$ (99.8%), Bi_2O_3 (99.975%), TiO_2 (99.6%), and ZnO (99.99%) (all Alfa Aesar) were milled in ethanol at 250 rpm for 12 h. The powders were calcined at 850-900 °C for 3 h with a heating rate of 5 K/min. After calcination, all the powders were remilled in ethanol at 250 rpm for 6 h. Subsequently, following a heating rate of 5 K/min, sintering was performed at 1150 °C for 3 h and 1050-1100 °C for 1 h for the undoped and doped compositions, respectively. The influence of quenching was selectively determined for 0.5 mole% Zn^{2+}-doped NBT100*y*BT (NBT100*y*BT-0.5), which were sintered at 1100 °C for a duration of 1 h and were directly taken out from the furnace and cooled in ambient air. These quenched samples are denoted as 0.5-Q1100. Sintered and quenched pellets were mechanically ground to a thickness of 0.4-0.6 mm and 7-8 mm in diameter. Annealing was performed for 30 min at 400 °C with a heating rate of 5 K/min to remove the mechanically induced strains that resulted from grinding.

Room-temperature X-ray diffraction (XRD) patterns for phase check were obtained in Bragg-Brentano geometry using

a Bruker D8 diffractometer with Cu-K$\alpha_{1,2}$ radiation. High-resolution datasets for Rietveld refinement were acquired from powders (obtained by crushing a pellet and annealing) in transmission geometry using a Stadi P (Stoe & Cie. GmbH) diffractometer equipped with MYTHEN1K (Dectris Ltd.) detector and monochromatized Cu-Kα_1 radiation ($\lambda = 1.540598$ Å, Ge[111]-monochromator) and analyzed using the FullProf suite.[44] The microstructures of samples polished down to 1/4 μm using diamond paste were imaged using scanning electron microscopy (Philips XL30 FEG) after thermally etching at 100-150 °C below the sintering temperature for 15 min. ^{23}Na magic angle spinning (MAS) Nuclear Magnetic Resonance (NMR) spectra were recorded with a Bruker Avance III 600 MHz spectrometer. Rectangular bar-shaped samples were spun with spinning frequencies between 6 and 7.5 kHz in a 4 mm MAS probe tuned at 158.75 MHz. NMR spectra were collected using single-pulse experiments with a pulse length of 0.75 μs, a recycle delay of 2 s and a dwell time of 0.1 μs. MAS results in both a spinning sideband envelope (SSE) and a center band (CB) and afford quantification of the cubic phase fraction of the material.[45,46]

For all the electrical measurements, sintered pellets were ground and electroded with Ag. Poling was done at 6 kV/mm for 15 minutes. The permittivity measurements were carried out using a HP analyzer interfaced with a furnace in the temperature regime from ambient temperature to 500 °C with a heating rate of 2 K/min. Polarization (P-E) and strain (S-E) hysteresis loops were recorded with a triangular field at a frequency of 1 Hz using a Sawyer-Tower circuit coupled with an optical sensor. Resonance measurements using the 3dB method[47] were performed on poled samples using an impedance analyzer (Alpha-Analyzer, Novocontrol). The sub-coercive ac field dependence of permittivity was determined using an impedance analyzer (Alpha-Analyzer, Novocontrol) interfaced with a high voltage unit (HVB 300, Novocontrol). The piezoelectric coefficient between room temperature and 225 °C was measured in situ with a heating rate of 2 K/min, using the converse piezoelectric effect, with a Polytec VDD-E-600 Vibrometer Front-End and a Polytec OFV-505 Sensor.[48] The direct piezoelectric coefficient was determined using a Berlincourt-d_{33}-meter (PM300, Piezotest).

3 | PHASE PURITY AND MICROSTRUCTURE

X-ray diffraction patterns ascertain that all the samples exhibit single-phase perovskite structure (Figure S1 provides exemplary graphs). The substitution of Zn^{2+} in NBT100*y*BT lowers the sintering temperature and dwell time, suggesting that Zn^{2+} acts as a sintering aid, which is further confirmed by the increase in grain size, also typical for acceptor-doped materials. Dense microstructures with a relative density of 96-98% were obtained (Figure S2). Furthermore, quenching preserves the microstructural features that results from doping (Figure S2 b,d,f,h).

4 | THERMAL DEPOLARIZATION AND EVIDENCE OF SPONTANEOUS FERROELECTRIC ORDER

4.1 | Small-signal dielectric and piezoelectric measurements

The thermal evolution of the poled permittivity (ε') at 10 kHz for the doped and 0.5-Q1100 samples of NBT6BT and NBT9BT are depicted in Figure 1. The frequency-dependent permittivity and dielectric loss (tan δ) in the poled and unpoled state are presented in Figures S3 and S4. In the case of non-ergodic relaxor

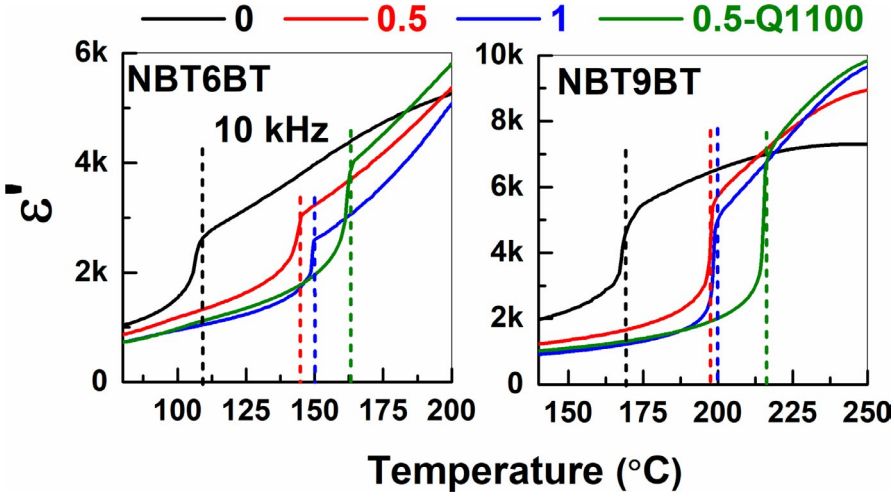

FIGURE 1 Temperature-dependent permittivity for doped and 0.5-Q1100 samples of NBT6BT and NBT9BT in the poled state at 10 kHz. T_{F-R} is marked with dotted lines. [Color figure can be viewed at wileyonlinelibrary.com]

Sample	mole % Zn^{2+}	$\Delta\varepsilon_p$(%)	$\Delta\varepsilon_{Hz}$ (%)	tan δ (unpoled)	$T_{F\text{-}R}$, °C (poled)	T_d, °C (poled)	γ
NBT6BT	0	56	18	0.06	104	105	1.89
	0.5	56	9	0.02	143	137	1.79
	1	54	4.5	0.01	150	148	1.69
	0.5-Q1100	61	11	0.02	166	163	1.80
NBT9BT	0	17	21	0.05	169	169	1.78
	0.5	5	5	0.01	196	194	1.68
	1	5	3	0.01	196	196	1.63
	0.5-Q1100	5.6	5	0.01	213	215	1.61

TABLE 1 Characteristic physical quantities extracted from Figures 1-2 and Figures S3-S4. $\Delta\varepsilon_p$ was evaluated as the difference in the permittivity in the poled and unpoled state at 40 °C at 10 kHz normalized to the permittivity in the unpoled state. $\Delta\varepsilon_{Hz}$ was evaluated as the difference in the unpoled permittivity between 10 kHz and 1 MHz, normalized to the permittivity at 10 kHz at 40 °C.

compositions of poled NBT100*y*BT, the first anomaly in the temperature- and frequency-dependent dielectric spectra corresponds to the ferroelectric-relaxor transformation temperature ($T_{F\text{-}R}$) and the second anomaly is commonly referred to as T_m, signifying the maximum in permittivity.[49] The thermal depolarization is dictated by $T_{F\text{-}R}$ for NBT100*y*BT, wherein, the domain structure randomizes prior to the disruption of long-range ordered ferroelectricity.[50] It is evident from Figure 1 that $T_{F\text{-}R}$ increases with increasing Zn^{2+} dopant concentration for both NBT6BT and NBT9BT as quantified in Table 1.

For NBT6BT-0.5, $T_{F\text{-}R}$ increases by 40 °C. In the prior work on Zn^{2+}-doping[15], the change in $T_{F\text{-}R}$ is the same as reported here except for the difference in the doping concentration, which can be attributed to the sensitivity of NBT to the Na^+ and Bi^{3+} concentration, since they are volatile. For NBT9BT-0.5, $T_{F\text{-}R}$ increases to 196 °C (Table 1). A further increase in $T_{F\text{-}R}$ by 15-17 °C is observed for 0.5-Q1100 (Table 1). Although the dielectric loss (tan δ) increases significantly for the doped and 0.5-Q1100 samples at high temperatures (Figures S3 and S4), the losses at room temperature are lower than their undoped counterparts (Table 1). For 1 mole% Zn^{2+}-doped NBT6BT and NBT9BT, the $T_{F\text{-}R}$ does not significantly increase further than that of 0.5 mole % Zn^{2+}-doped materials. It may be tempting to attribute this to be due to the solid solubility limit of Zn^{2+} in NBT-BT; however, note that no noticeable secondary phases were observed in the microstructure (Figure S2); also, the grain size increases notably for 1 mole % Zn^{2+}-doped compositions, typical of acceptor-doped materials and in contradiction with the context of solid solubility limit. This can be further investigated based on the critical limit of dopant concentration; however, such explorations are beyond the scope of this study.

A characteristic feature of relaxor materials is the frequency dispersion observed in the dielectric spectra, which is evaluated by considering the normalized difference in the unpoled permittivity measured at 10 kHz and 1 MHz, expressed in %. ($\Delta\varepsilon_{Hz}$ in Table 1).[51] $\Delta\varepsilon_{Hz}$ decreases with increasing Zn^{2+} concentration. Classical ferroelectrics exhibit changes in permittivity in the poled and unpoled state, attributed to the change in the number density of interfaces (domain walls, phase boundaries, etc.).[52,53] In the case of non-ergodic relaxors, the lower permittivity in the poled state can be rationalized to be due to the reduction in the high domain wall density (Polar nano regions grow into large-sized ferroelectric domains). This implies that larger differences in the permittivity between the poled and unpoled states directly correlate with strong relaxor features. This normalized difference, $\Delta\varepsilon_p$ is expressed in % (Table 1). The higher values of $\Delta\varepsilon_p$ indicate that NBT6BT exhibits stronger relaxor features in comparison to NBT9BT. The largest changes in $\Delta\varepsilon_p$ and $\Delta\varepsilon_{Hz}$ are observed for NBT6BT - 56% and 18%, respectively, and in comparison, these values are 17% and 21%, respectively, for NBT9BT. Furthermore, doped compositions of NBT9BT exhibit a decreasing trend in both $\Delta\varepsilon_p$ and $\Delta\varepsilon_{Hz}$. Note that the difference in permittivity is relatively small for the doped compositions of NBT9BT. In comparison, although doped compositions of NBT6BT exhibit a decrease in $\Delta\varepsilon_{Hz}$, $\Delta\varepsilon_p$ remains largely unaltered, indicating relaxor features. The relatively small changes in $\Delta\varepsilon_p$ and $\Delta\varepsilon_{Hz}$ (3-5.6 %) for doped and 0.5-Q1100 samples of NBT9BT reflect the absence of frequency dispersion in the unpoled permittivity response (Figure S4f-h, $\Delta\varepsilon_{Hz}$ in Table 1). Note that strong frequency dispersion is observed for NBT9BT (Figure S4e, $\Delta\varepsilon_{Hz}$ in Table 1). This is an indication for the development of a spontaneous (in the absence of external stimuli) ferroelectric order in the doped and 0.5-Q1100 samples of NBT9BT, as also noted recently in quenched NBT9BT[29] and the composite NBT9BT:ZnO.[54] From the previously reported work on the NBT6BT:ZnO composites, one can infer a similar trend exemplified by the absence of frequency dispersion for NBT6BT:0.3ZnO (10.78 vol.% ZnO) in the unpoled state.[17] The doped compositions of NBT6BT exhibit significantly larger values of $\Delta\varepsilon_p$ than that for Zn^{2+}-doped NBT9BT. The 0.5-Q1100 samples feature $\Delta\varepsilon_p$ and $\Delta\varepsilon_{Hz}$ close to that of the doped counterparts. A modified Curie-Weiss fit[55] of these compositions confirms this premise of stabilization of ferroelectric order. From the diffuseness parameters γ in Table 1, two inferences are

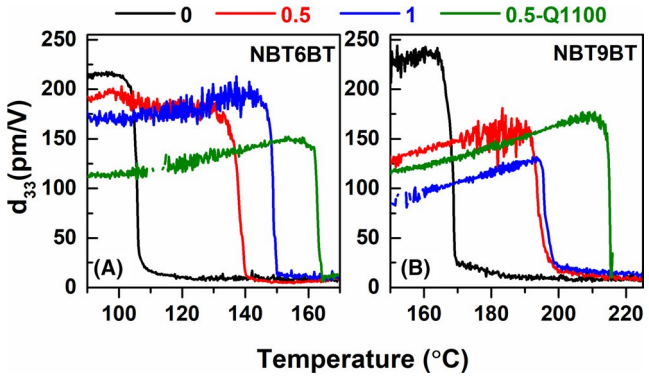

FIGURE 2 Temperature-dependent d_{33} measured from poled samples. [Color figure can be viewed at wileyonlinelibrary.com]

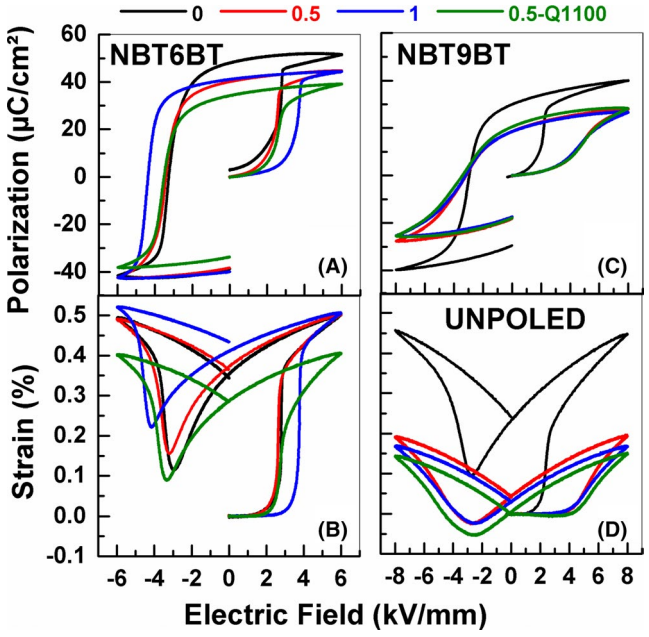

FIGURE 3 (A,C) Polarization- and (B,D) strain- field hysteresis obtained in the virgin state. [Color figure can be viewed at wileyonlinelibrary.com]

made- a) NBT6BT (γ=1.89) exhibits stronger relaxor characteristics as opposed to NBT9BT (γ=1.78) and b) doped and 0.5-Q1100 samples exhibit a decreasing trend in γ, implying a tendency towards stabilizing a ferroelectric state. This tendency is much stronger for doped NBT9BT compositions, with the lowest γ (1.61) for NBT9BT-0.5-Q1100.

The doped and 0.5-Q1100 samples of NBT6BT and NBT9BT feature a decreasing trend in d_{33} (Figure 2), the details of which are discussed in section 5.1. All the compositions exhibit a sharp decrease in d_{33} close to $T_{F\text{-}R}$. T_d established from these measurements closely mimics the $T_{F\text{-}R}$ determined from the temperature-dependent permittivity of poled samples. The inflection point at which d_{33} drops to zero is denoted as T_d in Table 1.

The sharp decrease in d_{33} (T) is unlike the case of the composites of NBT6BT with ZnO inclusions, which demonstrated a gradual decay of d_{33} with increasing volume fraction of ZnO.[25] The depolarization behavior of NBT6BT-0.5 is comparable to the composite NBT6BT:0.1ZnO (3.87 vol. % ZnO)[25] and quenched NBT6BT.[29]

4.2 | Large signal hysteresis measurements in the virgin state

The non-ergodic relaxor compositions of NBT100*y*BT undergo a relaxor to ferroelectric transformation upon application of electric field[56] or stress[57], which results in large electromechanical strains[58] and the corresponding change in the structure from average pseudocubic symmetry to a mixture of tetragonal and rhombohedral phases.[10] Therefore, the strain-field hysteresis in the virgin state provides a quick insight into the nature of this transformation in the doped and 0.5-Q1100 samples of NBT100*y*BT. Figure 3 depicts the polarization- and strain-field hysteresis measured in the virgin state of the samples.

The transformation strain ($S_{R\text{-}F}$) is defined as the maximum strain observed in the first cycle of the applied electric field (to a virgin sample) and the equivalent in the polarization-field hysteresis is the total polarization (P_{tot}). Note that the undoped NBT6BT and NBT9BT compositions exhibit a large $S_{R\text{-}F}$ of 0.52 % and 0.43 %, respectively (Table 2). A decreasing trend in $S_{R\text{-}F}$ and P_{tot} is observed with increasing dopant concentration. The decrease in $S_{R\text{-}F}$ and P_{tot} is 4%

TABLE 2 Piezoelectric coefficient (d_{33}) and characteristic quantities extracted from hysteresis measurements. The total polarization (P_{tot}), transformation strain ($S_{R\text{-}F}$), and transformation field ($E_{R\text{-}F}$) are extracted from the data plotted in Figure 3.

	mole % Zn^{2+}	d_{33}, pC/N	P_{tot}, μC/cm²	$S_{R\text{-}F}$, %	$E_{R\text{-}F}$, kV/mm
NBT6BT	0	138±10	49±3	0.52±0.02	3±0.02
	0.5	125±10	44±1	0.50±0.02	2.85±0.3
	1	115±5	44±1	0.47±0.04	3.69±0.4
	0.5-Q1100	105±5	39±2	0.39±0.02	3.29±0.3
NBT9BT	0	140±10	40±1	0.43±0.02	2.5±0.2
	0.5	98±5	30±2	0.20±0.03	4.9±0.5
	1	95±5	25±3	0.15±0.02	5.1±1
	0.5-Q1100	88±5	28±1	0.17±0.02	3.8±0.06

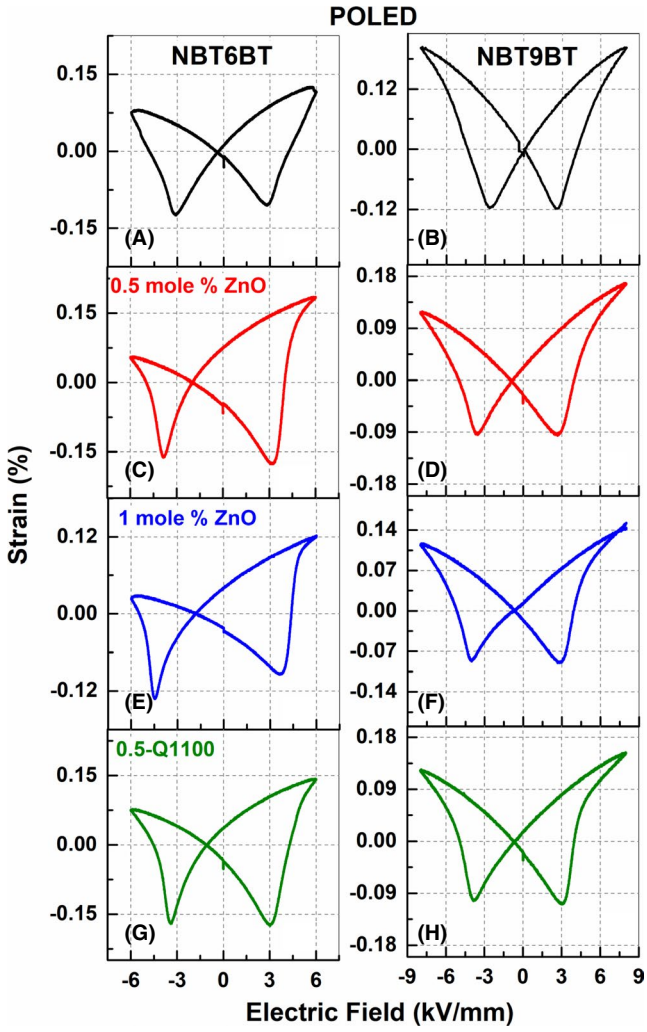

FIGURE 4 Strain-field hysteresis obtained in the poled state. The grid lines are guides to track the shift of the loops along the abscissae. [Color figure can be viewed at wileyonlinelibrary.com]

and 10%, respectively, for NBT6BT-0.5. The corresponding changes are 53% and 25% for NBT9BT-0.5 (Table 2). Furthermore, note the differences in the strain-field hysteresis in Figure 3D - the large increase in strain observed for NBT9BT is absent for the doped and 0.5-Q1100 samples. The inflection point at which the strain increases corresponds to the onset of long-range ferroelectric order ($E_{R\text{-}F}$). $E_{R\text{-}F}$ of NBT9BT-0.5 is twice that of NBT9BT. The prior work on quenching also established that the onset of ferroelectric order resulted in a decrease in $S_{R\text{-}F}$ and an increase in $E_{R\text{-}F}$ for the virgin strain-field hysteresis response.[29] Based on the above, it is inferred that the relaxor to ferroelectric transformation is absent in NBT9BT-0.5. A similar observation is made for NBT9BT-0.5-Q1100 and NBT9BT-1Zn. These samples also exhibited no frequency dispersion in the permittivity response (Figure S4 f-h and Table 1), as discussed previously in section 4.1. Hence, it can be concluded that doped and 0.5-Q1100 samples of NBT9BT spontaneously develop a ferroelectric order, akin to quenched NBT9BT [29] and composite NBT9BT:ZnO.[54] The doped compositions of NBT6BT also exhibit a decreasing trend in the $S_{R\text{-}F}$ and P_{tot} and an increasing trend in $E_{R\text{-}F}$, albeit, unlike the marked changes as in the case of NBT9BT. This trend is also comparable to the NBT6BT:ZnO composites, wherein the $S_{R\text{-}F}$ and $E_{R\text{-}F}$ were demonstrated to decrease and increase, respectively, with increasing volume fraction of ZnO.[59] NBT6BT-0.5-Q1100 exhibits further decrease in P_{tot} and $E_{R\text{-}F}$ in comparison to NBT6BT-0.5, indicating a higher propensity to stabilize the ferroelectric order in the system. These results correlate well to the premise of a stabilized ferroelectric order in NBT6BT-0.5-Q1100 (reflected as a further increase in $T_{F\text{-}R}$ upon quenching the doped sample).

5 | ELECTROMECHANICAL HARDENING

Considering the potential of NBT-based materials to replace $Pb(Zr,Ti)O_3$ in ultrasonic applications[3], it is imperative to investigate the electromechanical hardening in the Zn^{2+}-doped and 0.5-Q1100 samples of NBT100*y*BT. Acceptor-doping typically results in increased oxygen vacancy concentration, in order to maintain charge neutrality. The increased defect concentration act on their own as mobile defects or combine with other cation defects and form defect dipoles.[60,61] These, in turn, constrain the movement of domain walls, thus limiting the reorientation of domains upon application of electric field. This manifests as a decrease in the piezoelectric coefficient and an increase in the mechanical quality factor.[62] Another direct evidence of the hardening of the electromechanical properties is the development of an internal bias field (E_{ib}), which is observed from the shift of the hysteresis loops along the abscissae.

5.1 | Piezoelectric and ferroelectric properties in the poled state

The piezoelectric coefficient, d_{33}, decreases with increasing dopant concentration (Table 2). A 10% decrease in d_{33} is observed for NBT6BT-0.5; the corresponding change is 30% for NBT9BT-0.5. In comparison, the composite NBT6BT:0.1ZnO (3.87 vol. % ZnO) exhibited a 12% decrease in d_{33}.[11] A further 10-15% decrease in the piezoelectric coefficient is observed for 0.5-Q1100 in comparison to the doped samples. These results are the first indications of hardening effects due to Zn^{2+}-doping at the B-site of NBT100*y*BT.

Saturated bipolar strain-field hysteresis from poled samples was obtained for NBT6BT materials (undoped, doped, and 0.5-Q1100) at 6 kV/mm (Figure 4). Note that the maximum field required for saturation of the hysteresis response is higher, at 8 kV/mm, for the doped and 0.5-Q1100 samples of

NBT9BT, which is close to the breakdown field (Figure S5). The loops are not saturated for an applied field of 6 kV/mm for 1 mole % Zn^{2+}-doped NBT9BT (Figure S5). The strain-field hysteresis loops of NBT6BT materials (Figure 4A-D) reveal stronger asymmetry compared to NBT9BT materials (Figure 4E-H). Furthermore, both strain- as well as polarization- field loops (Figure 4 and S6) are strongly shifted in the x-axis for NBT6BT materials in comparison to NBT9BT materials.

The shift of the loops along the abscissae is quantified by the internal bias field (E_{ib}).[23] E_{ib} for NBT6BT-0.5 exhibits a twofold increase to -0.4 kV/mm in comparison to NBT6BT. In contrast, 1 mole % Fe-doped NBT6BT exhibits E_{ib} close to zero and increases to -0.1 kV/mm after aging at room temperature for $2x10^5$ s.[23] In the case of NBT9BT, E_{ib} is zero within the limits of error and increases to -0.4 kV/mm for NBT9BT-0.5. E_{ib} does not alter much for both NBT6BT and NBT9BT with further increase in the dopant concentration and for 0.5-Q1100.

The hysteresis losses (normalized maximum width of the hysteresis loop) decrease from 27% for NBT6BT to 15% for NBT6BT-0.5 (Figure 5). NBT9BT materials (doped and 0.5-Q1100) do not feature such a drastic change in the hysteresis losses (Figure 5). The twofold increase in E_{ib} and reduction in the hysteresis losses by ~ 12% are similar to that reported for the composite NBT6BT:0.1ZnO (3.87 vol. % ZnO, E_{ib} = -0.35 kV/mm and hysteresis losses = 15%).[11]

The doped compositions of NBT6BT and NBT9BT exhibit clear indications of electromechanical hardening as reflected in the decrease in d_{33} (Table 2), reduced hysteresis losses and increase in E_{ib} (Table 3). A further decrease in d_{33} is observed for 0.5-Q1100; however, the hysteresis losses and E_{ib} are comparable to their doped counterparts.

5.2 | Mechanical quality factor and Rayleigh coefficient

NBT6BT-0.5 and NBT6BT-1 exhibit mechanical quality factor $Q_{m,res}$ of 287 and 627, respectively (Table 3), which is roughly a two- and four- fold increase in comparison with NBT6BT ($Q_{m,res}$ = 130). A twofold increase in the mechanical quality factor is also observed for NBT9BT-0.5 ($Q_{m,res}$ = 152) in comparison with NBT9BT ($Q_{m,res}$ = 75). However, further increase in dopant concentration does not improve the quality factor in NBT9BT. This result corroborates with that for the E_{ib} and the hysteresis losses discussed in section 5.1. The mechanical quality factor of 0.5-Q1100 does not improve further as a result of quenching and is comparable to those obtained for the doped samples. $Q_{m,anti}$ evaluated from the antiresonant part of the impedance spectra is also tabulated in Table 3 and exhibits a similar trend to $Q_{m,res}$. Note that the choice of starting NBT100*y*BT composition is crucial. While doping NBT9BT is beneficial in increasing T_{F-R} close to 200 °C, the increment in quality factor, albeit significant, is comparable to that of pure NBT6BT; also, d_{33} decreases drastically in doped NBT9BT in comparison to that of NBT6BT. Therefore, comparing core-MPB (NBT6BT) and end-member-MPB (NBT9BT) relaxor compositions, it can be established that the core-MPB relaxors are a better choice for the doping strategy. Contrasting to comparable NBT-based hard piezoceramics[3,41,63] ascertains that NBT-6BT-1 exhibits the highest mechanical quality factor.

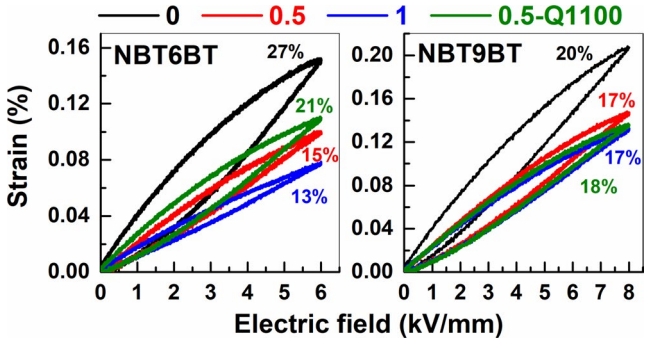

FIGURE 5 Unipolar strain-field hysteresis obtained in the poled state. The numbers indicate the hysteresis losses.

The Rayleigh relationship is used to elucidate the electromechanical hardening effects that result due to Zn^{2+}-doping.[11,64] Since domain wall mobility is constrained in "hard-type" piezoelectrics, the Rayleigh coefficient α is typically lower. Indeed, α decreases by 80% for NBT6BT-0.5 in comparison to NBT6BT (Table 3) and is further lowered for NBT6BT-1. A 90 % reduction in α was reported previously for the composite NBT6BT:0.1ZnO (3.87 vol. % ZnO). NBT9BT-0.5 exhibits a 65% decrease in α and remains the same with a further increase in Zn^{2+}-dopant concentration. Quenching the doped compositions does not induce further changes in α, similar to the trend in mechanical quality factor.

From the above, it can be inferred that the hardening effects are more pronounced for Zn^{2+}-doping in the core-MPB composition (NBT6BT) as opposed to the MPB end-member compositions (NBT9BT). Although 0.5-Q1100 samples exhibit enhanced T_{F-R} in comparison with the doped counterparts, the electromechanical hardening effects are not significantly altered upon quenching. Nevertheless, it can be concluded that Zn^{2+} is an effective acceptor dopant to electromechanically hardening NBT6BT.

6 | ELECTRICAL CONDUCTIVITY

The Nyquist plots of impedance in Figure S7 indicate a single process of the bulk conductivity response for the undoped compositions. In the case of doped and 0.5-Q1100 samples, the semicircular response indicates two processes, plausibly

TABLE 3 Characteristic quantities indicating electromechanical hardening. The internal bias field (E_{ib}) and hysteresis loss are evaluated from the data plotted in Figures 4 and 5, respectively. Mechanical quality factors (Q_{res} and Q_{anti}) are calculated from resonance measurements. Rayleigh coefficient (α) is obtained from the linear fits of permittivity as a function of the electric field. The activation energy (E_a) is obtained from the linear fit of the data plotted in Figure 6. The complete description of the activation energies at different temperature regimes is tabulated in Table S1.

	Zn-mole %	-E_{ib} (kV/mm)	Hysteresis loss (%)	$Q_{m, res}$	$Q_{m, anti}$	α (mm/kV)	High E_a (eV)
NBT6BT	0	0.16±0.09	27±1	130±20	179±40	60±20	1.25
	0.5	0.4±0.15	15±1	287±45	360±90	12±3	0.53
	1	0.4±0.1	13±1	627±20	987±47	8±3	0.61
	0.5-Q1100	0.3±0.1	21±1	280±40	395±28	11±3	0.58
NBT9BT	0	0	20±1	75±15	77±45	31±10	1.23
	0.5	0.4±0.1	17±1	152±44	183±13	11±2	0.59
	1	0.4±0.1	17±1	156±39	187±57	10±3	0.57
	0.5-Q1100	0.4±0.1	18±1	127±20	177±76	10±2	0.57

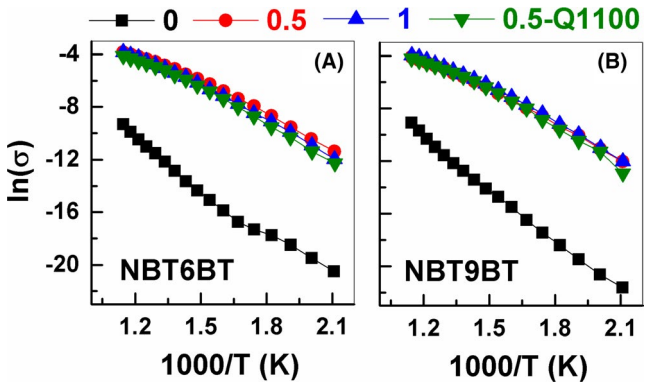

FIGURE 6 Arrhenius plots of conductivity evaluated from impedance measurements depicted in Figure S7. [Color figure can be viewed at wileyonlinelibrary.com]

indicating a phase mixture with distinct electrical properties. Note the two orders of magnitude decrease in the scaling, which indicates enhanced conductivity for the doped compositions (Figure S7).

The plot of conductivity as a function of temperature in Figure 6 is used to quantify the activation energies (E_a), which can denote the ionic/electronic conduction in the system.[65] In accordance with prior reports from Li et al.,[65] two different slopes can be obtained (Figure 6) depending on the temperature regime of interest which corresponds to high and low E_a(Table S1). The activation energies with values close to half the band gap of NBT100*y*BT (3.25 eV[12]) indicate dominant ionic contributions to the conductivity.[65] E_a is in the range of 0.72-0.85 eV for NBT6BT (undoped, doped, and 0.5-1100) in the low-temperature regime (Table 3, S1). The corresponding values for NBT9BT are 1.09 eV for the undoped sample and ~0.8 eV for the doped and 0.5-Q1100 samples of NBT9BT. E_a in the high-temperature regime obtained from linear fits of the data in Figure 6 is tabulated in Table 3. In the case of undoped samples, E_a in the high-temperature regime is ~1.25 eV for both NBT6BT and NBT9BT, which is close to roughly half the band gap of these materials.[66] Further, the absence of electrode polarization behavior at low frequencies (Figure S7) confirms predominant electronic conductivity at all temperatures. The doped and 0.5-Q1100 samples of both NBT6BT and NBT9BT exhibit E_a in the range of 0.5-0.6 eV at high temperatures. These values are closer to that at low temperatures (0.8 eV), as stated in Table S1. In comparison, Mg-doped NBT exhibits E_a in the range of 0.37-0.61.[66] Therefore, the doped and 0.5-Q1100 samples exhibit dominant ionic contributions at all temperatures. The conductivities of 0.5-Q1100 samples does not differ much from their doped counterparts. This is attributed to doping providing a much higher oxygen vacancy concentration, which experiences relatively small changes upon quenching.[28,29] Note the negligible changes in the resistance of the doped (0.5 and 1) and 0.5-Q1100 samples compared in Figure S7 and in the temperature-dependent conductivity plotted in Figure 6. This result directly corroborates the negligible electromechanical hardening effects in 0.5-Q1100 samples in comparison with their doped counterparts.

7 | STRUCTURE-PROPERTY CORRELATION

High-resolution X-ray diffraction profiles of undoped and doped NBT100*y*BT powders in the unpoled state are plotted for comparison in Figure 7. NBT6BT-0.5 features deviations from the cubic symmetry as indicated by the presence of additional reflections, highlighted by arrows (Figure 7 A,B). "pc" denotes pseudocubic indexing. Note that the splitting in both 111_{pc} and 200_{pc} indicates a mixture of rhombohedral and tetragonal phases (Figure 7B). These additional reflections in 200_{pc} are absent for undoped NBT6BT; a closer look at 111_{pc} indicates three reflections and therefore suggests a phase mixture of cubic and rhombohedral phases, as reported previously.[16] NBT6BT is usually refined with a *R*3*c* structural model; however, since the

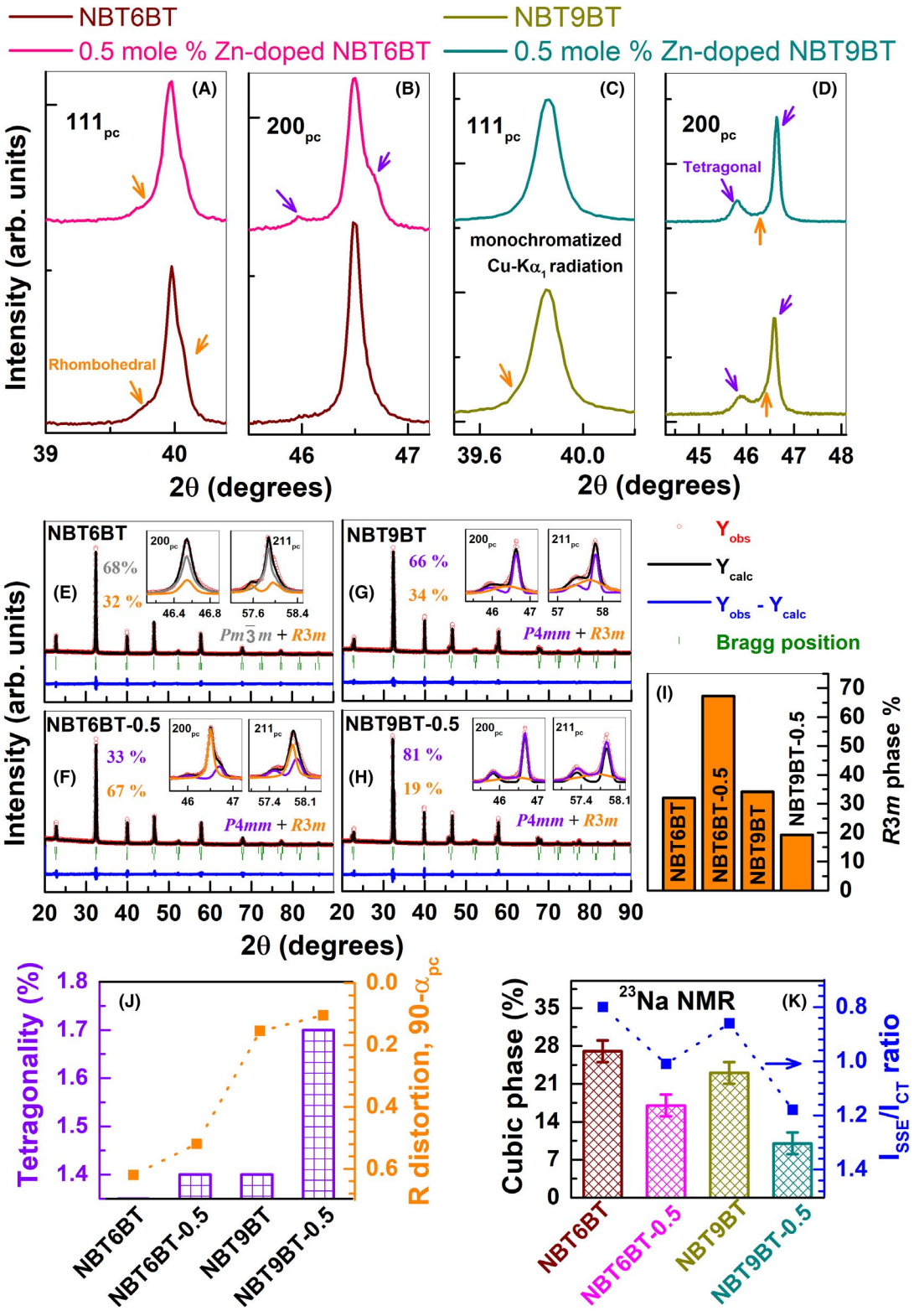

FIGURE 7 (A-D) High-resolution X-ray diffraction profiles obtained using monochromatized Cu-Kα_1 radiation (λ = 1.540598 Å, Ge[111]-monochromator) from unpoled powder samples obtained by crushing and annealing a sintered pellet. The arrows indicate the characteristic signature of the tetragonal and rhombohedral phases. (E-H) Rietveld refinement fits of the high-resolution diffraction dataset. The insets highlight the fits of some of the pseudocubic (pc) Bragg profiles. The Bragg positions are depicted by vertical lines (green color) - the top one corresponds to the *Pm*$\bar{3}$*m* or *P4mm* phase and the bottom one corresponds to the *R3m* phase. The calculated profiles in the inset are marked for the *Pm*$\bar{3}$*m* (gray), *P4mm* (violet), and *R3m* (orange) phases. (I) *R3m* phase fraction and (J) unit cell distortions for the respective phases established from Rietveld fits. The tetragonality is evaluated as (c/a-1)*100. The rhombohedral (R) distortion is evaluated as 90-α_{pc} (K) Relative amount of cubic phase (bars) and I_{SSE}/I_{CB} ratio (solid squares) established from ^{23}Na NMR experiments. [Color figure can be viewed at wileyonlinelibrary.com]

superlattice reflections corresponding to the $a^-a^-a^-$ tilt were not observed in this dataset, the structural model was chosen as *R*3*m* (rhombohedral) in accordance with previous reports.[10] *Pm*3*m* was used to refine the cubic phase. In the case of NBT9BT (Figure 7 C,D), the diffraction profiles indicate clear splits in 200_{pc} corresponding to the tetragonal phase. The intensity profile between the two tetragonal splits and broadened 111_{pc} reflections in comparison to NBT6BT indicate the presence of an additional phase, most likely of rhombohedral nature. Previous literature reports indicate that NBT100*y*BT compositions with higher $BaTiO_3$ content exhibit *P*4*mm* symmetry.[56,67] Hence, a *P*4*mm*+*R*3*m* structural model was used to fit NBT9BT and NBT9BT-0.5. The refined fits are displayed in Figure 7 (E-H) and the refined structural parameters are tabulated in Table S2. The difference profiles (Figure 7E-H) and reliability factors (Table S2) confirm the goodness of fit. In the case of NBT6BT-0.5, apart from the development of a tetragonal distortion, the *R*3*m* phase fraction increases to 67 %, while in NBT9BT-0.5, the *R*3*m* phase fraction decreases to 19 % (Table S2, Figure 7I). Correspondingly, the rhombohedral distortion decreases for the doped compositions in comparison with their undoped counterparts. Note that the rhombohedral distortion also changes from ~0.6 to ~0.15 with a change in $BaTiO_3$ content for both doped and undoped compositions (Table S2, Figure 7J). This plausibly indicates an *R*3*c* to *R*3*m* crossover. Such a crossover with increasing $BaTiO_3$ content has been reported previously.[67]

The key feature of Zn^{2+}-doping in NBT100*y*BT is the development of a tetragonal phase and the enhanced unit cell distortion. Note that with the development of the tetragonal phase in NBT6BT-0.5, the tetragonal distortion of this composition becomes comparable to NBT9BT at 1.4 % (Table S2, Figure 7J). Furthermore, the tetragonality for NBT9BT-0.5 increases to 1.7 %.

The non-ergodic NBT100*y*BT relaxors can be modeled as a simple system consisting of polar (non-cubic) nanoregions in an isotropic (cubic) matrix phase in the unpoled state.[45] Therefore, a stabilization of the ferroelectric order would implicate the development of non-cubic distortions and should result in a decreased cubic content. ^{23}Na NMR has been previously employed to quantify the cubic phase fraction in NBT100*y*BT and could also establish the changes in the cubic phase fraction (ex situ) upon application of electric field.[45] Figure S8 provides the ^{23}Na MAS NMR spectra of unpoled, undoped NBT6BT and NBT9BT followed by the samples doped with 0.5% mole of Zn^{2+}. Note that the relative intensity of the SSE increases upon doping. The intensity ratio between the two spectral components (I_{SSE}/I_{CB}) is 1.5 for a sample that displays solely a non-cubic local symmetry around the sodium nuclei. Conversely, a value smaller than 1.5 is observed whenever a cubic phase fraction is present. The cubic content obtained from unpoled samples using ^{23}Na NMR is plotted in Figure 7K and tabulated in Table S2. It decreases from ~25 % in the undoped samples to 17 % and 10 % for NBT6BT-0.5 and NBT9BT-0.5, respectively. In comparison, the cubic content for the composite NBT6BT:0.1ZnO (3.87 vol. % ZnO) composite was previously determined as 11%.[25] Although, NBT9BT-0.5 indicated a development of spontaneous ferroelectric order from the absence of frequency dispersion in the permittivity response (Figure S4f) and reduced $S_{R\text{-}F}$ (Figure 3D, Table 2), note that the cubic content of NBT9BT-0.5 is still considerable at 10%, indicating the existence of local polar heterogeneities; however, this is lower than that of NBT6BT-0.5. Recall that NBT6BT-0.5 exhibited strong frequency dispersion in comparison to NBT9BT-0.5 (Table 1) and the cubic phase fractions correlate well to this trend. Also, the increase in non-cubic phase fraction directly correlates to the development of the tetragonal phase as established from diffraction investigations.

8 | CONCLUSIONS

Zn^{2+}-doping has been proven to be beneficial in enhancing both the thermal stability of the piezoelectric response and electromechanically harden two different NBT100*y*BT compositions. The highest increase in $T_{F\text{-}R}$ is established for 0.5 mole % Zn^{2+}-doped NBT9BT at 196 °C, which further increases to 213 °C upon quenching. The best properties are achieved for 1 mole % Zn^{2+}-doped NBT6BT, with $T_{F\text{-}R}$ of 150 °C and a mechanical quality factor of 627. The doped compositions exhibit predominantly ionic conductivity as established from impedance spectroscopy. Quenching the doped compositions increases the $T_{F\text{-}R}$ further by ~17 °C, however, does not significantly alter the electromechanical properties and the conductivity. The enhanced thermal stability is rationalized based on the stabilization of ferroelectric order, supported by the stabilization of a tetragonal phase.

ACKNOWLEDGMENTS

Lalitha K.V. thanks Prof. Wolfgang Donner for access to the different powder diffractometers with a monochromatic source and J.C. Jaud for enabling the experiments. Lalitha K.V. thanks Prof. Oliver Clemens for providing access to the laboratory X-ray diffractometer with Cu-K$\alpha_{1,2}$ source and Aamir Iqbal Waidha for enabling the experiments. Lalitha K.V. thanks Prof. Gerd Buntkowsky for providing access to the NMR spectrometer. Lalitha K.V. acknowledges and thanks the Alexander von Humboldt Foundation and the Deutsche Forschungsgemeinschaft under grant no. KO 5948/1-1 (Nr. 414311761) for financial support. MPS and PBG gratefully acknowledge financial support by the Deutsche Forschungsgemeinschaft through project Grant No. BU 911/28-1. Open access funding enabled and organized by Projekt DEAL.

ORCID

Lalitha Kodumudi Venkataraman https://orcid.org/0000-0002-4848-5436
Aamir Iqbal Waidha https://orcid.org/0000-0002-4554-8470
Pedro B. Groszewicz https://orcid.org/0000-0002-5246-6449
Jürgen Rödel https://orcid.org/0000-0002-8975-7741

REFERENCES

1. Rödel J, Webber KG, Dittmer R, Jo W, Kimura M, Damjanovic D. Transferring lead-free piezoelectric ceramics into application. J Eur Ceram Soc. 2015;35:1659–89.
2. Bell AJ, Deubzer O. Lead-free piezoelectrics—The environmental and regulatory issues. MRS Bull. 2018;43:581–7.
3. Tou T, Hamaguti Y, Maida Y, Yamamori H, Takahashi K, Terashima Y. Properties of $(Bi_{0.5}Na_{0.5})TiO_3$–$BaTiO_3$–$(Bi_{0.5}Na_{0.5})(Mn_{1/3}Nb_{2/3})O_3$ Lead-Free Piezoelectric Ceramics and Its Application to Ultrasonic Cleaner. Jpn J Appl Phys. 2009;48:7GM03.
4. Doshida Y, Shimizu H, Mizuno Y, Tamura H. Investigation of high-power properties of $(Bi,Na,Ba)TiO_3$ and $(Sr,Ca)_2NaNb_5O_{15}$ piezoelectric ceramics. Jpn J Appl Phys. 2013;52:7HE01.
5. Takenaka T, Sakata K. Dielectric, piezoelectric and pyroelectric properties of $(BiNa)_{1/2}TiO_3$- based ceramics. Ferroelectrics. 1989;95:153–6.
6. Takenaka T, Sakata KO, Toda KO. Piezoelectric properties of $(Bi_{1/2}Na_{1/2})TiO_3$-based ceramics. Ferroelectrics. 1990;106:375–80.
7. Takenaka T, Maruyama K, Sakata K. $(Bi_{1/2}Na_{1/2})TiO_3$-$BaTiO_3$ system for lead-free piezoelectric ceramics. Jpn J Appl Phys. 1991;30:2236.
8. Shrout TR, Zhang SJ. Lead-free piezoelectric ceramics: alternatives for PZT? J Electroceramics. 2007;19:113–26.
9. Leontsev SO, Eitel RE. Progress in engineering high strain lead-free piezoelectric ceramics. Sci Technol Adv Mater. 2010;11:44302.
10. Hinterstein M, Schmitt LA, Hoelzel M, Jo W, Rödel J, Kleebe H-J, et al. Cyclic electric field response of morphotropic $Bi_{1/2}Na_{1/2}TiO_3$-$BaTiO_3$ piezoceramics. Appl Phys Lett. 2015;106:222904.
11. Lalitha KV, Riemer LM, Koruza J, Rödel J. Hardening of electromechanical properties in piezoceramics using a composite approach. Appl Phys Lett. 2017;111:22905.
12. Cernea M, Vasile BS, Capiani C, Ioncea A, Galassi C. Dielectric and piezoelectric behaviors of NBT-$BT_{0.05}$ processed by sol–gel method. J Eur Ceram Soc. 2012;32:133–9.
13. Davies M, Aksel E, Jones JL. Enhanced high-temperature piezoelectric coefficients and thermal stability of Fe- and Mn-substituted $Na_{0.5}Bi_{0.5}TiO_3$ ceramics. J Am Ceram Soc. 2011;94:1314–6.
14. Wang S-F, Tu C-S, Chang T-L, Chen P-Y, Chen C-S,Hugo Schmidt V, et al. Structural stability and depolarization of manganese-doped $(Bi_{0.5}Na_{0.5})_{1-x}Ba_xTiO_3$ relaxor ferroelectrics. J Appl Phys. 2014;116:154101.
15. Li L, Zhu M, Zhou K, Wei Q, Zheng M, Hou Y. Delayed thermal depolarization of $Bi_{0.5}Na_{0.5}TiO_3$-$BaTiO_3$ by doping acceptor Zn^{2+} with large ionic polarizability. J Appl Phys. 2017;122:204104.
16. Khatua DK, Mishra A, Kumar N, Adhikary GD, Shankar U, Majumdar B, et al. A coupled microstructural-structural mechanism governing thermal depolarization delay in $Na_{0.5}Bi_{0.5}TiO_3$-based piezoelectrics. Acta Mater. 2019;15:49–60.
17. Zhang J, Pan Z, Guo F-F, Liu W-C, Ning H, Chen YB, et al. Semiconductor/relaxor 0–3 type composites without thermal depolarization in $Bi_{0.5}Na_{0.5}TiO_3$-based lead-free piezoceramics. Nat Commun. 2015;19:6615.
18. Muramatsu H, Nagata H, Takenaka T. Quenching effects for piezoelectric properties on lead-free $(Bi_{1/2}Na_{1/2})TiO_3$ ceramics. Jpn J Appl Phys. 2016;55:10TB07.
19. Ren P, Wang J, Wang Y, Lalitha KV, Zhao G. Origin of enhanced depolarization temperature in quenched $Na_{0.5}Bi_{0.5}TiO_3$-$BaTiO_3$ ceramics. J Eur Ceram Soc. 2020;40:2964–9.
20. Li H, Feng C, Yao W. Some effects of different additives on dielectric and piezoelectric properties of $(Bi_{1/2}Na_{1/2})TiO_3$–$BaTiO_3$ morphotropic-phase-boundary composition. Mater Lett. 2004;58:1194–8.
21. Zhang Q, Zhang Y, Wang F, Wang Y, Lin D, Zhao X, et al. Enhanced piezoelectric and ferroelectric properties in Mn-doped $Na_{0.5}Bi_{0.5}TiO_3$–$BaTiO_3$ single crystals. Appl Phys Lett. 2009;95:102904.
22. Li J, Wang F, Leung CM, Or SW, Tang Y, Chen X, et al. Large strain response in acceptor- and donor-doped $Bi_{0.5}Na_{0.5}TiO_3$-based lead-free ceramics. J Mater Sci. 2011;46:5702.
23. Sapper E, Dittmer R, Damjanovic D, Erdem E, Keeble DJ, Jo W, et al. Aging in the relaxor and ferroelectric state of Fe-doped (1–x)$(Bi_{1/2}Na_{1/2})TiO_3$-x$BaTiO_3$ piezoelectric ceramics. J Appl Phys. 2014;116:104102.
24. Zhang H, Deng H, Chen C, Li L, Lin D, Li X, et al. Chemical nature of giant strain in Mn-doped $0.94(Na_{0.5}Bi_{0.5})TiO_3$–$0.06BaTiO_3$ lead-free ferroelectric single crystals. Scr Mater. 2014;15:50–3.
25. Riemer LM, Lalitha KV, Jiang X, Liu N, Dietz C, Stark RW, et al. Stress-induced phase transition in lead-free relaxor ferroelectric composites. Acta Mater. 2017;1:271–80.
26. Mahajan A, Zhang H, Wu J, Ramana EV, Reece MJ, Yan H. Effect of phase transitions on thermal depoling in lead-free $0.94(Bi_{0.5}Na_{0.5}TiO_3)$–$0.06(BaTiO_3)$ based piezoelectrics. J Phys Chem C. 2017;121:5709–18.
27. Fan Z, Zhou L, Kim T-H, Zhang J, Zhang S-T, Tan X. Mechanisms of enhanced thermal stability of polarization in lead-free (Bi1/2Na1/2)0.94Ba0.06TiO3/ZnO ceramic composites. Phys Rev Mater. 2019;3:24402.
28. Li Z-T, Liu H, Thong H-C, Xu Z, Zhang M-H, Yin J, et al. Enhanced temperature stability and defect mechanism of BNT-based lead-free piezoceramics investigated by a quenching process. Adv Electron Mater. 2018;5:1800756.
29. Lalitha KV, Koruza J, Rödel J. Propensity for spontaneous relaxor-ferroelectric transition in quenched $(Na_{1/2}Bi_{1/2})TiO_3$-$BaTiO_3$ compositions. Appl Phys Lett. 2018;113:252902.
30. Takagi Y, Nagata H, Takenaka T. Effects of quenching on bending strength and piezoelectric properties of $(Bi_{0.5}Na_{0.5})TiO_3$ ceramics. J Asian Ceram Soc. 2020;8:1–7.
31. Babu JB, He M, Zhang DF, Chen XL, Dhanasekaran R. Enhancement of ferroelectric properties of $Na_{1/2}Bi_{1/2}TiO_3$-$BaTiO_3$ single crystals by Ce dopings. Appl Phys Lett. 2007;90:102901.
32. Liu L, Zhu M, Hou Y, Yan H, Liu R. Abnormal piezoelectric and dielectric behavior of $0.92Na_{0.5}Bi_{0.5}TiO_3$-$0.08BaTiO_3$ induced by La doping. J Mater Res. 2007;22:1188–92.
33. Xiang P-H, Takeda H, Shiosaki T. Characterization of manganese-doped BaTiO3–$(Bi_{1/2}Na_{1/2})TiO_3$ positive temperature coefficient of resistivity ceramics using impedance spectroscopy. J Appl Phys. 2008;103:64102.

34. Ge W, Cao H, Li J, Viehland D, Zhang Q, Luo H. Influence of dc-bias on phase stability in Mn-doped $Na_{0.5}Bi_{0.5}TiO_3$-5.6 at. %$BaTiO_3$ single crystals. Appl Phys Lett. 2009;95:162903.
35. Xu M, Wang F, Wang T, Chen X, Tang Y, Shi W. Phase diagram and electric properties of the (Mn, K)-modified $Bi_{0.5}Na_{0.5}TiO_3$–$BaTiO_3$ lead-free ceramics. J Mater Sci. 2011;46:4675–82.
36. Erdem E, Schaab S, Jo W, Ozarowski A, Van Tol J, Eichel R-A. High-frequency EPR analysis of MnO_2 -Doped [$Bi_{0.5}$ $Na_{0.5}$]TiO_3-$BaTiO_3$ piezoelectric ceramics – manganese oxidation states and materials 'hardening'. Ferroelectrics. 2012;428:116–21.
37. Yao G, Wang X, Wu Y, Li L. Nb-Doped 0.9$BaTiO_3$–0.1($Bi_{0.5}Na_{0.5}$)TiO_3 ceramics with stable dielectric properties at high temperature. J Am Ceram Soc. 2012;95:614–8.
38. Glaum J, Simons H, Acosta M, Hoffman M. Tailoring the piezoelectric and relaxor properties of ($Bi_{1/2}Na_{1/2}$)TiO_3–$BaTiO_3$ via zirconium doping. J Am Ceram Soc. 2013;96:2881–6.
39. Guennou M, Savinov M, Drahokoupil J, Luo H, Hlinka J. Piezoelectric properties of tetragonal single-domain Mn-doped NBT-6 %BT single crystals. Appl Phys A. 2013;116:225–8.
40. Li-Ying L, Ru-Zhi W, Man-Kang Z, Yu-Dong H. Site occupation of doping La^3+ cations and phase transition in $Na_{0.5}Bi_{0.5}TiO_3$ -$BaTiO_3$ solid solution. Chin Phys B. 2013;22:36401.
41. Hu H, Zhu M, Xie F, Lei N, Chen J, Hou Y, et al. Effect of Co_2O_3 additive on structure and electrical properties of 85($Bi_{1/2}Na_{1/2}$)TiO_3–12($Bi_{1/2}K_{1/2}$)TiO_3–3$BaTiO_3$ lead-free piezoceramics. J Am Ceram Soc. 2009;92:2039–45.
42. Aksel E, Foronda H, Calhoun KA, Jones JL, Schaab S, Granzow T. Processing and properties of $Na_{0.5}Bi_{0.5}TiO_3$ piezoelectric ceramics modified with La, Mn and Fe. Funct Mater Lett. 2010;03:45–8.
43. Prasertpalichat S, Cann DP. Hardening in non-stoichiometric (1–x) Bi0.5Na0.5TiO3–xBaTiO3 lead-free piezoelectric ceramics. J Mater Sci. 2015;51:476–86.
44. Rodrigues Carvajal J. A Rietveld refinement and pattern matching analysis program, Laboratoire Leon Brillouin (CEA-CNRS). France. 2000.
45. Groszewicz PB, Breitzke H, Dittmer R, Sapper E, Jo W, Buntkowsky G, et al. Nanoscale phase quantification in lead-free ($Bi_{1/2}Na_{1/2}$)TiO_3-$BaTiO_3$ relaxor ferroelectrics by means of ^{23}Na NMR. Phys Rev B. 2014;90:220104.
46. Groszewicz PB, Gröting M, Breitzke H, Jo W, Albe K, Buntkowsky G, et al. Reconciling local structure disorder and the relaxor state in ($Bi_{1/2}Na_{1/2}$)TiO_3-$BaTiO_3$. Sci Rep. 2016;22:31739.
47. Uchino K, Zhuang Y, Ural SO. Loss determination methodology for a piezoelectric ceramic: new phenomenological theory and experimental proposals. J Adv Dielectr. 2011;01:17–31.
48. Leist T, Chen J, Jo W, Aulbach E, Suffner J, Rödel J. Temperature Dependence of the Piezoelectric Coefficient in $BiMeO_3$-$PbTiO_3$ (Me = Fe, Sc, ($Mg_{1/2}Ti_{1/2}$)) Ceramics. J Am Ceram Soc. 2012;95:711–5.
49. Jo W, Schaab S, Sapper E, Schmitt LA, Kleebe H-J, Bell AJ, et al. On the phase identity and its thermal evolution of lead free ($Bi_{1/2}Na_{1/2}$)TiO_3-6 mol% $BaTiO_3$. J Appl Phys. 2011;110:74106.
50. Jo W, Daniels J, Damjanovic D, Kleemann W, Rödel J. Two-stage processes of electrically induced-ferroelectric to relaxor transition in 0.94($Bi_{1/2}Na_{1/2}$)TiO_3-0.06$BaTiO_3$. Appl Phys Lett. 2013;102:192903.
51. Cross LE. Relaxor ferroelectrics. Ferroelectrics. 1987;76:241–67.
52. Lalitha KV, Kalyani AK, Ranjan R. Analogous stress and electric field driven structural transformation and decrease in polarization coherence on poling around the morphotropic phase boundary in $BiScO_3$-$PbTiO_3$. Phys Rev B. 2014;90:224107.
53. Kovaľ V, Briančin J. Effect of poling process on the piezoelectric and dielectric properties of Nb and Sr-doped PZT ceramics. Ferroelectrics. 1997;193:41–9.
54. Lalitha KV, Hinterstein M, Lee K-Y, Yang T, Chen L-Q, Groszewicz PB, et al. Spontaneous ferroelectric order in lead-free relaxor ($Na_{1/2}Bi_{1/2}$)TiO_3-based composites. Phys Rev B. 2020;101:174108.
55. Rivera I, Kumar A, Ortega N, Katiyar RS, Lushnikov S. Divide line between relaxor, diffused ferroelectric, ferroelectric and dielectric. Solid State Commun. 2009;149:172–6.
56. Ma C, Guo H, Beckman SP, Tan X. Creation and destruction of morphotropic phase boundaries through electrical poling: a case study of lead-free $Bi_{1/2}Na_{1/2}TiO_3$-$BaTiO_3$ piezoelectrics. Phys Rev Lett. 2012;109:107602.
57. Schader FH, Wang Z, Hinterstein M, Daniels JE, Webber KG. Stress-modulated relaxor-to-ferroelectric transition in lead-free ($Na_{1/2}Bi_{1/2}$)TiO_3-$BaTiO_3$ ferroelectrics. Phys Rev B. 2016;93:134111.
58. Jo W, Rödel J. Electric-field-induced volume change and room temperature phase stability of ($Bi_{1/2}Na_{1/2}$)TiO_3-x mol. % $BaTiO_3$ piezoceramics. Appl Phys Lett. 2011;99:42901.
59. Lalitha KV, Koruza J, Rödel J. Mechanical versus electromechanical hardening in relaxor ferroelectric $Na_{1/2}Bi_{1/2}TiO_3$-$BaTiO_3$ with ZnO inclusions. Scr Mater. 2019;1:92–5.
60. Arlt G, Neumann H. Internal bias in ferroelectric ceramics: origin and time dependence. Ferroelectrics. 1988;87:109–20.
61. Genenko YA, Glaum J, Hoffmann MJ, Albe K. Mechanisms of aging and fatigue in ferroelectrics. Mater Sci Eng B. 2015;192:52–82.
62. Damjanovic D. Ferroelectric, dielectric and piezoelectric properties of ferroelectric thin films and ceramics. Rep Prog Phys. 1998;61:1267.
63. Xu Q, Chen M, Chen W, Liu H-X, Kim B-H, Ahn B-K. Effect of CoO additive on structure and electrical properties of ($Na_{0.5}Bi_{0.5}$)0.93$Ba_{0.07}TiO_3$ ceramics prepared by the citrate method. Acta Mater. 2008;56:642–50.
64. Damjanovic D, Demartin M. The Rayleigh law in piezoelectric ceramics. J Phys Appl Phys. 1996;29:2057.
65. Li M, Pietrowski MJ, De Souza RA, Zhang H, Reaney IM, Cook SN, et al. A family of oxide ion conductors based on the ferroelectric perovskite $Na_{0.5}Bi_{0.5}TiO_3$. Nat Mater. 2014;13:31–5.
66. Seo I-T, Steiner S, Frömling T. The effect of A site non-stoichiometry on 0.94(Na_yBi_x)TiO_3-0.06$BaTiO_3$. J Eur Ceram Soc. 2017;37:1429–36.
67. Jo W, Daniels JE, Jones JL, Tan X, Thomas PA, Damjanovic D, et al. Evolving morphotropic phase boundary in lead-free ($Bi_{1/2}Na_{1/2}$)TiO_3–$BaTiO_3$ piezoceramics. J Appl Phys. 2011;109:14110.

SUPPORTING INFORMATION

Additional supporting information may be found online in the Supporting Information section.

How to cite this article: Kodumudi Venkataraman L, Zhu T, Pinto Salazar M, et al. Thermal depolarization and electromechanical hardening in Zn^{2+}-doped $Na_{1/2}Bi_{1/2}TiO_3$-$BaTiO_3$. *J Am Ceram Soc*. 2021;104: 2201–2212. https://doi.org/10.1111/jace.17581